ACES Asian Chemical Editorial Society

doi.org/10.1002/cnma.202300514

CHEMNANOMAT
Research Article

www.chemnanomat.org

Special Collection

Gold Microstructures by Thermolysis of Gold(III) Di-isopropyldithiocarbamate Complexes

A. Angeloski,*[a, b] K. Flower-Donaldson,[b, c] F. Matar,[b] D. C. Hayes,[b] M. N. Duman,[b] D. T. Oldfield,[d] M. T. Westerhausen,[e] and A. M. McDonagh[b]

Elemental gold was formed by thermolysis of gold(III) dithiocarbamate single-source precursors, which exist as two complexes. The complexes were readily synthesised from the reaction between chloroauric acid and sodium di-isopropyldithiocarbamate and could be isolated from each other. The thermal decomposition processes were evaluated using thermogravimetry and electrical resistance measurements. The structure and purity of the resultant gold was examined using scanning electron microscopy. The resultant gold materials were drastically different and dependent on the thermolysed complex.

Introduction

Single-source precursors (SSPs) have attracted significant and increasing attention due to their utility in the creation of a range of materials and structures.[1,2] In a chemical context, precursors are compounds that undergo a chemical reaction to produce other compounds. SSPs, therefore, are chemical compounds that contain all of the required elements (i.e., a single source) to make target compounds or materials. SSPs remove the requirement to perform complex or interfering chemical reactions at the sites where materials are to be deposited. Furthermore, modifications can be made to reactant stoichiometry, thermal properties, chemical structures, as well as external parameters such as heating rates and environments to facilitate control over the morphology and composition of the resultant target materials.[3]

Metal complexes bearing dithiocarbamate (DTC) ligands have been extensively investigated as SSPs for materials including a range of metal sulfide compounds.[1,3–23] Dithiocarbamate ligands provide useful and accessible building blocks; the flexibility to readily engineer and alter the dithiocarbamate ligand allows a range of coordination complexes to be generated.[3,5–30] In addition, numerous metal dithiocarbamate complexes have been extensively studied in the area of crystal growth and design and thus there exists a depth of structural understanding.[26–28]

Metallic gold is a very useful material but there are few examples of gold SSPs. Existing SSPs for metallic gold materials include tetrachloroauric acid and complexes employing triphenylphosphine and trifluoromethyl stabilising ligands.[31—38] There are also examples of gold(III) dithiocarbamate complexes that have been used as SSPs for the growth of gold films using chemical vapour deposition.[39—43] The most established of these is dimethyl-diethyldithiocarbamato gold(III), which is a volatile gold(III) complex used in the deposition of gold films by thermal decomposition on surfaces.[39—41] However, some synthetic challenges include the use of dimethyl gold(III) iodide, which is typically a low yielding product of organometallic Grignard reactions,[44] and their volatility limits their use as solid-state SSPs for the formation of gold microstructures.

Of particular relevance to the current work, gold(III) di-isopropyldithiocarbamate (Au(DIPDTC)) complexes exist as two compounds with distinct structural motifs in systems bearing one or two DTC ligands.[45–47] These complexes are not air or water sensitive, extremely straightforward to synthesise from the reaction between gold(III) chloride and sodium di-isopropyldithiocarbamate under aqueous conditions, and require little purification. The ease of synthesis and the ability of these dichloride complexes to be easily purified, when compared to their dialkyl derivatives offers several advantages such as reduced cost, time to prepare, and an increased accessibility due to less complicated synthetic procedures. In our recent work we have demonstrated the use of metal di-isopropyldi-

[a] Dr. A. Angeloski
National Deuteration Facility, Australian Nuclear Science Technology Organisation, Sydney, NSW, Australia,
E-mail: angelosa@ansto.gov.au

[b] Dr. A. Angeloski, K. Flower-Donaldson, F. Matar, D. C. Hayes, M. N. Duman, Assoc. Prof. A. M. McDonagh
School of Mathematical and Physical Sciences, University of Technology Sydney, NSW, Australia

[c] K. Flower-Donaldson
Minerals, Australian Nuclear Science Technology Organisation, Sydney, NSW, Australia

[d] Dr. D. T. Oldfield
Nuclear Materials Development and Characterisation, Australian Nuclear Science Technology Organisation, Sydney, NSW, Australia

[e] Dr. M. T. Westerhausen
Hyphenated Mass Spectrometry Laboratory, University of Technology Sydney, NSW, Australia

Supporting information for this article is available on the WWW under https://doi.org/10.1002/cnma.202300514

Special Collection This manuscript is a contribution to a Joint Early Career Researcher Special Collection published by Chemistry – An Asian Journal, ChemNanoMat and the Asian Journal of Organic Chemistry.

thiocarbamate complexes as solid-state SSPs to produce nano and sub-micron sized metal sulfide materials.[5,6, 48] We have also demonstrated the mechanisms for their decomposition.[5] Thus, we believe that Au(DIPDTC) complexes would behave as SSPs for the formation of metallic gold, and that differences in the SSP structure may lead to different morphologies in the metallic gold materials.

Here we investigate the use of gold(III) di-isopropyldithiocarbamate complexes, which exist in multiple structural forms, as SSPs for the formation of metallic gold structures.[47] We employed solid- and solution-state techniques to track the formation of gold(III) di-isopropyldithiocarbamate complexes from the initial reaction between metal and ligand to the isolation of individual crystals. NMR spectroscopy, optical photomicroscopy and single-crystal X-ray diffraction were definitive in demonstrating the structural differences. We used mass spectrometry to characterise the composition of the volatile species upon thermal decomposition of the gold (III) di-isopropyldithiocarbamate complexes and demonstrate that these materials form metallic gold microcrystals upon thermal decomposition.

Results and Discussion

Compounds **1** and **2** were synthesised by reacting aqueous $HAuCl_4$ and NaDIPDTC (Scheme 1). Analysis of the reaction product revealed the presence of both **1** and **2**, with a large excess of **1**. The relative amount of **2** could be increased by heating an acetone solution of the reaction mixture at reflux for 72 hr. Pure **1** and **2** were obtained by fractional crystallisation, and their structures were confirmed by comparison of lattice constants to previously determined structures using single-crystal X-ray diffraction (Table S1).[47]

Videography using cross-polarised photomicroscopy (Videos S**1** and S**2**) during evaporation of acetone solutions of **1** and **2** was used to examine the crystallisation process. Complete solvent evaporation occurred in ~15 minutes, leading to the growth of crystals with **1** crystallising as plates and **2** crystallising as needles (Figure 1). In both cases, only a single morphology of crystals was produced, with no appearance of **2** in the growth of **1**, or **1** in the growth of **2**. This indicates that any conversion between **1** and **2** is very slow relative to the period of crystal growth. Crystals of **1** and **2** were simultaneously observed when an acetone solution of crude reaction mixture (i.e. containing both **1** and **2**) was crystallised.

Solution state ^{1}H NMR spectra of **1** and **2** were distinguishable from each other, with the methyl and methine protons appearing ~0.05 ppm higher in **1** than **2**, which is attributed to a slightly reduced electronic density about the -NCS_2 moiety in the bis-substituted cationic gold complex **1** when compared to the neutral dichloro **2** (Figure 1).

Thermogravimetric analysis data of **1** and **2** are shown in Figure 2 and Figure 4. For both **1** and **2** there was no mass loss in the 50–150 °C region indicating a lack of water (bound or otherwise), in agreement with the crystallographic data.[47] There is a small (<3%) mass loss before 200 °C that produced isopropylisothiocyanate from trace amounts of surface-adhered sodium di-isopropyldithiocarbamate ligand. Thermal decomposition of **1** occurs in three distinct events. The first event occurs between 190 and 215 °C and a mass loss of 13% which we assign to the loss of three chlorine atoms from the $[AuCl_4]^-$ anion to form AuCl (*calc.* 12%). This mass loss likely represents the loss of elemental chlorine (which subsequently forms HCl) as evidenced by the lack of any ions with m/z >50 detected between ~190–210 °C (Figure 2). The presence of trace residual atmosphere was confirmed by the detection of SO_2 (m/z 64.1) which is produced by oxidation of sulfur-containing volatile species. The loss of chlorine at these temperatures is in agreement with literature describing the thermal decomposition of $AuCl_4^-$ moieties.[49] The second event occurs steadily between 215 and 250 °C with a mass loss of 14% which we assign to complete loss of chlorine from the anionic AuCl component to yield elemental gold[49] and partial fragmentation of the dithiocarbamato cationic component losing isopropylisothiocyanate (*calc.* 15%) as determined by the high abundance of ions with m/z 101.2 corresponding to the mass loss event. The loss of isopropylisothiocyanate is a well-established mech-

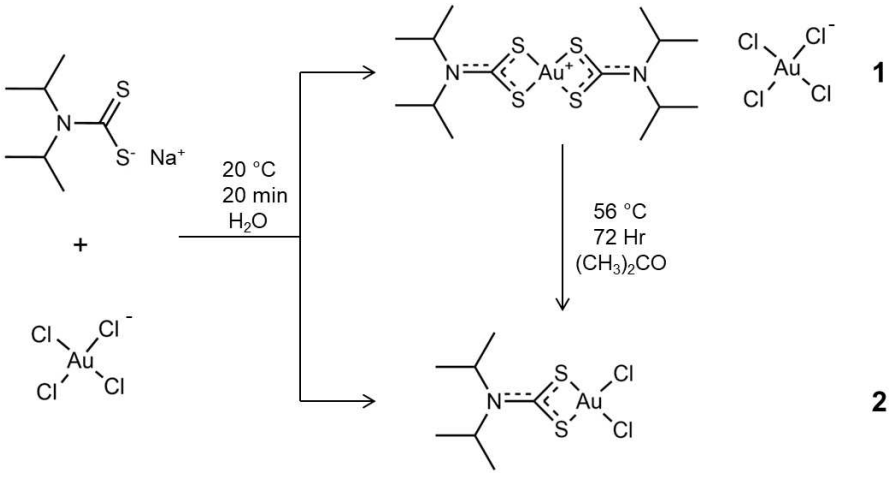

Scheme 1. Synthesis of **1** and **2**.

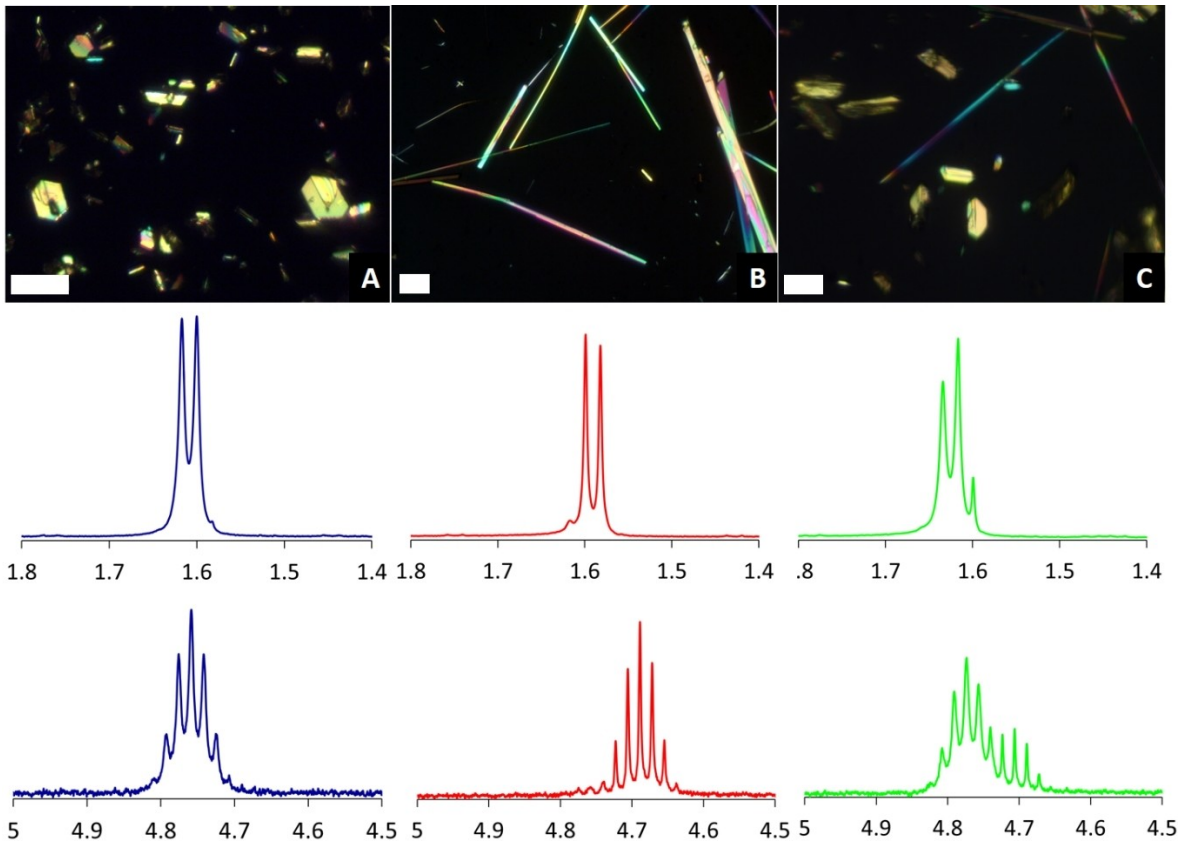

Figure 1. Photomicrographs (upper) using cross polarised light showing the morphology of **1** (A) and **2** (B) isolated from the reaction mixture, and crystallisation of **1** and **2** from the untreated reaction mixture (Scale bar = 50 μm). ^{1}H NMR spectra of the solutions used to produce the crystals (lower) is shown.

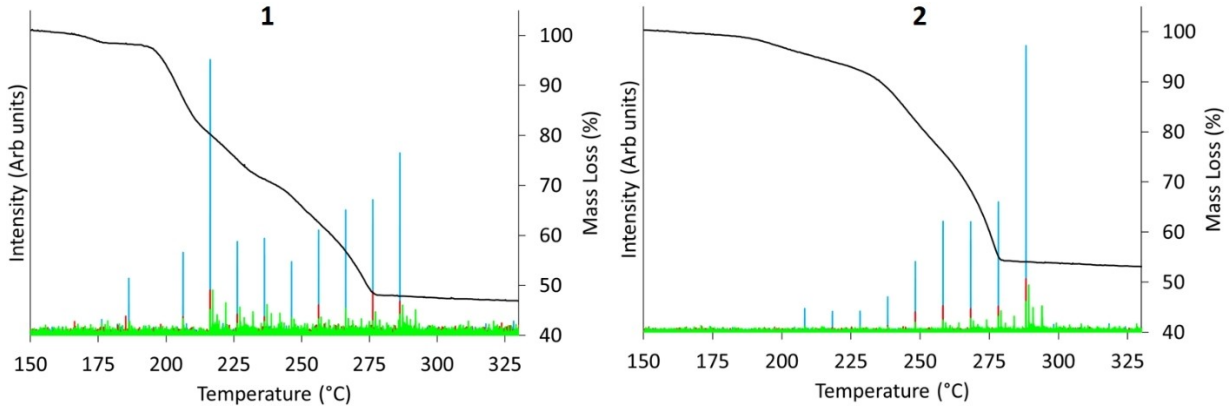

Figure 2. Thermogravimetric data for **1** and **2** showing evolution of volatile species: m/z 101.2 (blue), 78 (red) and 64.1 (green). *Note the offset between mass loss and volatile species is due to a 10 minute delay between MS injections.

anism for the thermal cleavage of di-isopropyldithiocarbamato complexes at the metal-sulfur and dithiocarbamato sulfur-carbon bonds.[5] Thermal degradation of the dithiocarbamato cationic component is associated with an increase in the abundance of m/z 78, which represents the formation of 2-chloropropane. The presence of 2-chloropropane is further evidence for the fate of the chloride during thermolysis. In di-isopropyldithiocarbamate complexes lacking chloride, propene evolution was observed.[5] When chlorine is evolved, it reacts with residual atmosphere producing HCl that subsequently undergoes an addition reaction with propene to produce 2-chloropropane. Decomposition of the remaining dithiocarbamate cationic component occurs between 250 and 280 °C and a mass loss of 26% to produce a residue of 47% which is assigned to the complete removal of all remaining dithiocarbamato and sulfur as isopropylisothiocyanate. These residual masses are in good agreement with the expected mass of reduced metallic gold (*calc.* 44.3%) as the final product.

Thermal decomposition of **2** occurs in one broad event between 200 and 275 °C and a mass loss of 55 % which we assign to a complete loss of the dithiocarbamate and chloride ligands leading to formation of reduced metallic gold (*calc* 55.7 %). The di-isopropyldithiocarbamate ligand simultaneously produces isoropylisothiocyanate and 2-chloropropane during this thermal decomposition event. The marked differences in thermal behaviour between **1** and **2** is attributed to the presence of an anionic $[AuCl_4]^-$ component in **1**, which is absent in **2**. That the decomposition of the anion occurs *before* loss of co-ordinated DTC indicates that the square planar AuS_4 moiety is more stable than $[AuCl_4]^-$. Observations reported for polynuclear and heteropolynuclear di-isopropyldithiocarbamate complexes of gold are in agreement with the current data.[46,47,50] These thermal decomposition mechanisms are not equivalent to those of di-alkyldithiocarbamato gold (III) complexes which evolve the dithiocarbamate ligand intact without any fragmentation;[39,40] the fragmentation of the di-isopropyldithiocarbamate ligands in **1** and **2** during thermolysis demonstrates the relative strength of the AuS_4 and AuS_2Cl_2 moieties when compared to their dialkyl derivatives.

The thermal decomposition products were examined using SEM (Figure 3). Thermal decomposition was halted at temperatures corresponding to thermal decomposition events as determined using thermogravimetric analysis to allow for visual characterisation of intermediate microstructures (Figure S1). The residues formed by complete thermolysis of **1** and **2** are distinctly different (Figure 3C and D). After the first decomposition step at ~220 °C, partially thermally decomposed **1** is visually identified and confirmed *via* EDX (Figure S2) as a residue which encompasses ~1 μm sized facetted gold microcrystals (Figure 3A and B, Figure S3). Focussed ion beam (FIB) milling of these intermediate gold microcrystals (Figure S4) reveals a solid gold interior structure and thus demonstrates the formation of solid gold microcrystals during partial decomposition of **1** at 230 °C. At 300 °C no unreacted **1** remains

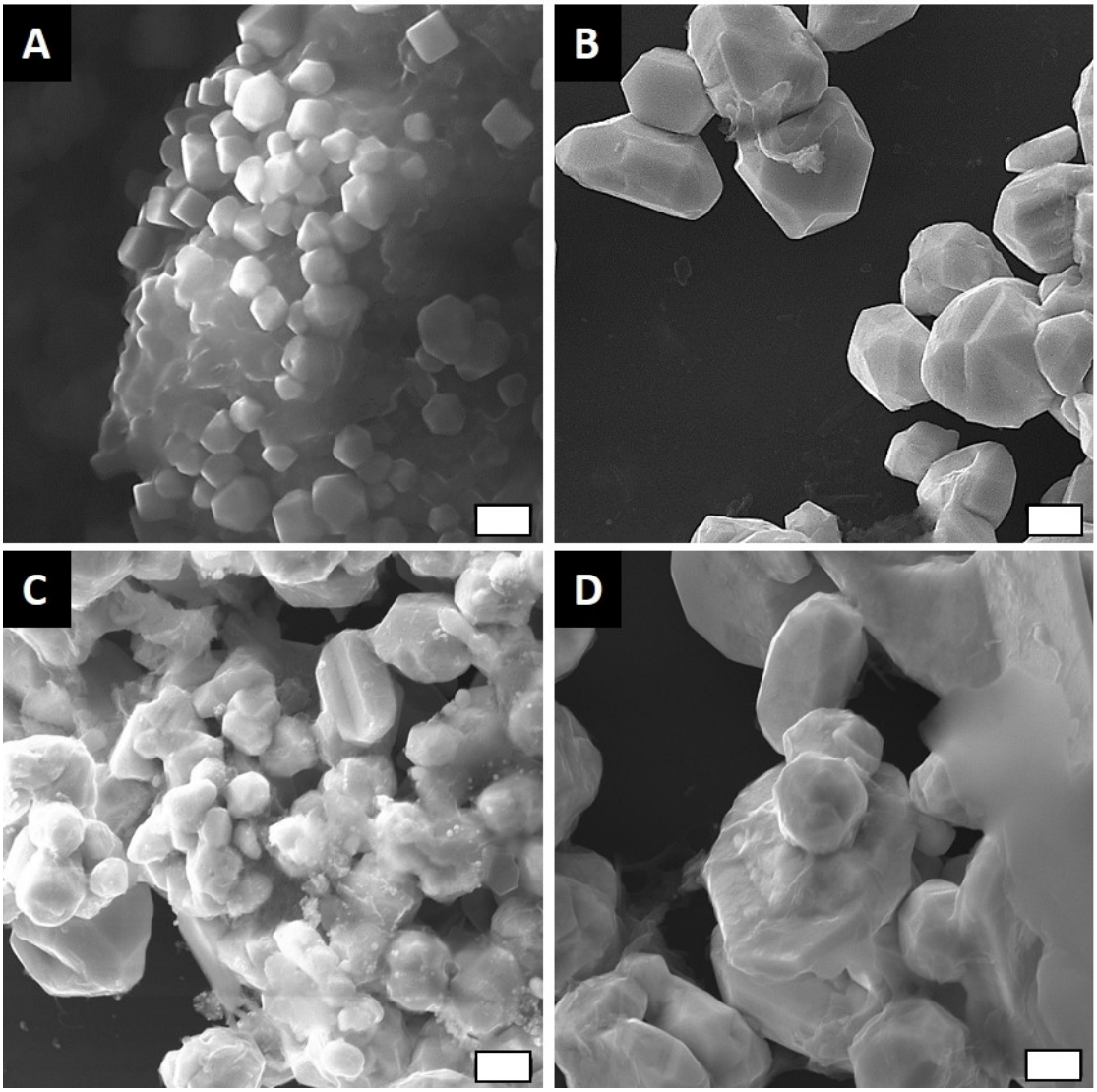

Figure 3. SE SEM photomicrographs showing intermediate gold microcrystals formed during thermolysis of **1** (230 °C, A and B) and the final microstructures after complete thermolysis of **1** and **2** (300 °C, C and D). The field of view in all images is 5 μm and the scale bars are 500 nm.

(as confirmed using EDX, Figure S5) and the resultant microstructured gold is observed as a mixture of larger micron-sized facetted crystals dispersed amongst smaller clusters of gold (Figure 3C). Above 300 °C, the crystalline gold remains consistent in size but undergoes a 'smoothing' or loss of morphology (Figure S1, D). These 'smoothed' gold microcrystals are chemically pure gold (as determined using EDX, Figure S6) and produced a solid gold interior structure when milled by a FIB (Figure S7). Thermal decomposition of **2** predominately produces ~1–5 μm sized plates of gold (Figure 3D, Figure S1 E–F, Figures S8-9) with very little faceted gold microcrystals observed. Above the temperature at which all **2** has decomposed, the plates merge to form a somewhat connected microstructure of globular gold.

Consideration of the thermogravimetric analysis is informative; the formation of gold from thermal decomposition of the $[AuCl_4]^-$ anion in the case of **1** is clearly demonstrated by the observation of well-defined gold facetted microcrystals dispersed in the dithiocarbamato component of **1** at 230 °C (Figure 3A–B, Figure S1A–B). The size of these microcrystals is ~10x larger than those typically produced from the decomposition of $[AuCl_4]^-$ alone,[35,37,38,51] and their morphology is in agreement with twinned plate and icosahedral geometries typically observed when gold is grown on nanoclustered gold seeds.[36,52] At 230 °C, the amount of **1** visually decreases in agreement with the thermogravimetry whilst the relative abundance of the microcrystalline gold structures increases. At 300 °C, no further decomposition occurred and only gold microcrystals remained. The formation of only one type of morphology can be explained as follows; thermal decomposition of $[AuCl_4]^-$ at ~230 °C produced solid micron sized gold crystals which seeded further growth of gold from the subsequent decomposition of the dithiocarbamato gold moiety. In the case of **2**, the abundance of facetted gold microcrystals is extremely low and the microstructures are dominated by plate-like crystals. We attribute this to the formation of gold from the single-step decomposition of the dithiocarbamatogold(III) complex. As there is no $[AuCl_4]^-$ present, there cannot be formation of gold before the thermal decomposition of the dithiocarbamato complex and thus there is no morphology to seed the further growth of gold, leading to the observation of plates. Our findings are supported by previous thermolysis studies of other metal DTC complexes,[5,6] where well-defined microstructures were observed during crystal growth from a matrix of partially decomposed dithiocarbamato components. When crystal growth occurred from the solid phase directly, plate-like morphologies were observed.

To gain further insight into the thermal decomposition and formation of microstructured gold, variable temperature resistance measurements were performed using interdigitated gold electrodes. Samples of **1** and **2** were heated in an argon atmosphere and the results are displayed in Figure 4. In both cases, the materials did not produce an intermediate solution phase, rather, decomposition occurred directly from the solid state in two events for **1** and one event for **2** (Videos S3 and S4).

For **1** and **2**, the resistance of the powdered material prior to thermolysis was >100 MΩ. There were initial reductions in resistance to ~1 MΩ during a region of ≤ 1% mass loss, which we attribute to liberation of trace adsorbed organic species as observed by the presence of isopropylisothiocyanate at equivalent temperatures (Figure 2) leading to a measurable increase in conductivity. For **1**, the formation of ionic chloride species and AuCl (as discussed previously) results in an ~15× increase in conductivity (~1.3 MΩ→~87 KΩ) during the mass loss event initiated at ~200 °C. The formation of intermediate gold microstructures as shown in Figure 3 is reflected by a second dramatic increase in conductivity from ~87 KΩ to ~140 Ω which occurs at ~230 °C and further supports the assignment of complete thermal decomposition of the $[AuCl_4]^-$ anion to yield a suspension of gold microcrystals in a matrix of dithiocarbamatogold(III) residue (Figure 3A); these gold microcrystals reach a percolation threshold and form a continuous conductive contact spanning the inter-electrode surface, thus lowering the resistance near to that of pure gold. Time-lapsed photography of this decomposition event shows clearly the formation of a dark black/brown residue which is attributed to the suspended gold microcrystals (Video S3). The complete thermal decomposition of the dithiocarbamato residues to yield pure gold (Figure S10) is indicated by the final drop in resistance to 30 Ω which is observed at ~280 °C.

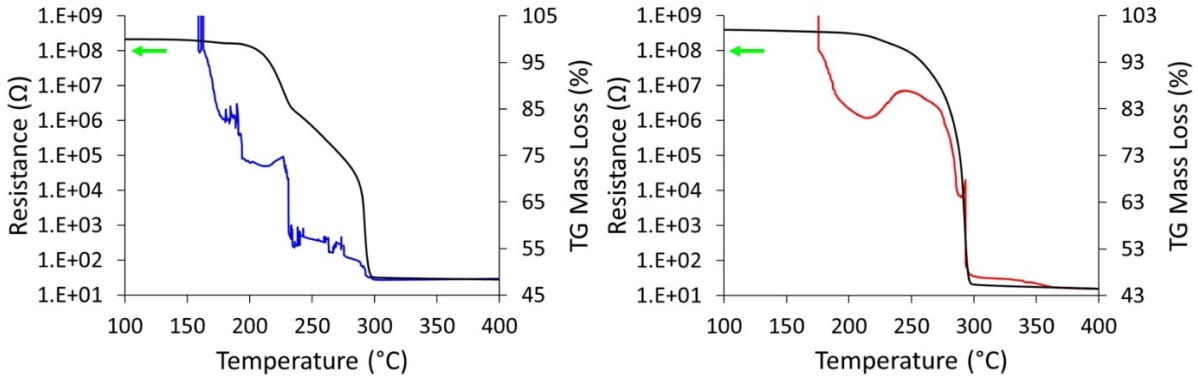

Figure 4. Resistance data for thermal decomposition of **1** (blue trace) and **2** (red trace) during heating in an argon atmosphere. Thermogravimetric data at an equivalent heating rate of 10 °C min^{-1} (black line) is shown for context. The green arrow represents the maximum resistance measurable by our instrument.

In contrast, for **2** there are no intermediate drastic decreases in resistance as observed for **1**; the precipitous decrease in resistivity is not observed until the complete thermal decomposition of the dithiocarbamate complex in a single step initiated at ~280 °C, which leads to the formation of metallic gold (Figure 4 and Figure S8). The increasing conductivity during thermal decomposition of **1** and **2** is consistent with the SEM data and thermogravimetric analysis; i.e. **1** decomposes partially into elemental gold microstructures which seed the further growth of elemental gold during decomposition of the dithiocarbamate moiety, whereas **2** decomposes in a single rapid event forming plates. In both cases, the decomposition of the precursors formed a continuous mass of gold spanning at least $>50\ \mu m$ (Figure S10). The stark differences in thermal behaviour are also supported by time-lapsed photography (Videos S3 and S4).

Conclusions

Two gold(III) di-isopropyldithiocarbamate complexes produced metallic gold microcrystals upon thermolysis. The decomposition of these compounds was analysed using thermal, chromatographic, and electrical resistance techniques which showed differences in the thermolysis regime. The precursors produced isopropylisothiocyanate and 2-chloropropene as the dominant thermal decomposition products. For **1**, the thermolysis occurred in two events and produced intermediate dodecahedral gold microcrystals, observed using SEM and manifested as a drastic decrease in electrical resistance during thermal decomposition, whereas for **2** the thermolysis occurred in one step and produced a plate-like gold microcrystalline material with no intermediate gold microcrystals being observed. The formation of an intermediate microstructured gold material during thermolysis of **1** is important as it highlights an opportunity to isolate microstructured gold materials that cannot be obtained by the decomposition of $[AuCl_4]^-$ alone.

Experimental

General

Sodium di-isopropyldithiocarbamate and chloroauric acid were prepared using literature methods.[48,53] All other chemicals and reagents were purchased from Merck, Sigma-Aldrich, or Chem Supply and used as received. Solution state nuclear magnetic resonance spectroscopy was performed using a Bruker Avance III spectrometer and $(CD_3)_2CO$ as the solvent. The frequency for ^1H was 400.15 MHz and 100.63 MHz for ^{13}C. Thermal analysis was performed using a Netzsch STA 449 F5 Jupiter thermal analyser. Alumina crucibles (90 μL) were charged with samples and experiments were conducted using an atmosphere of 99.9995% helium. A heating rate of 1 °C min^{-1} was employed between 35 and 400 °C. Simultaneous Gas Chromatography-Mass Spectrometry was performed using a heated transfer line from the furnace to an Agilent 7890/5977 Gas Chromatography-Mass Spectrometer. A ~250 μL aliquot of furnace atmosphere was automatically sampled in 10 °C increments and diluted 1:5 with 99.9995% helium prior to injection through an Agilent HP-5MS column. Seperation of volatiles was achieved with an isothermal temperature of 200 °C. This setup thus produces a total ion chromatograph every 10 °C during thermal decomposition. Mass spectra were obtained with a *m/z* range of 50 to 400 amu, and referenced to known fragmentation patterns using a NIST 2014 database (NIST 14).

Single crystals were selected under a Leica M165Z polarizing microscope and mounted on MicroMount consisting of a thin polymer tip with a wicking aperture. The X-ray diffraction measurements were carried out on a Bruker D8 Quest Single Cystal diffractometer with a Photon II detector at 120 K by using IμS 3.0 Microfocus Source with Mo–Kα radiation ($\lambda = 0.710723$ Å). The single crystal, mounted on the goniometer using cryo loops for intensity measurements, was coated with paraffin oil and then quickly transferred to the cold stream using an Oxford Cryo stream 800 attachment. The raw frames were background corrected, fitted, and integrated using CrysAlis Pro. The lattice constants were compared to the previous determined structures.[47] High resolution mass spectrometry (HRMS) was performed using a Shimadzu 9050 time of flight spectrometer operating in rapid-polarity switching mode at 100 Hz scan rate with a mobile phase of 70% acetonitrile, 30% water, and a flow rate of 0.4 mL min^{-1}. Fourier transform infrared (FTIR) spectra were acquired using a Nicolet 6700 FTIR spectrometer fitted with a diamond smart iTX ATR accessory. Ultraviolet-Visible absorbance spectra (UV-VIS) were acquired using a custom-made fibre-optic spectroscopy system (Avantes) and samples were illuminated with a modified W/D_2 source (Heraeus FibreLight D_2).

Synthesis

Sodium di-isopropyldithiocarbamate (0.799 g, 2.76 mmol) was dissolved in 20 mL of Milli-Q water, to which one mole equivalent of $HAuCl_4$ (0.939 g, 2.76 mmol) dissolved in 20 mL of Milli-Q was added dropwise. The reaction was performed at room temperature and mixed for 20 minutes once the entirety of the $HAuCl_4$ had been added. The yellow solution on addition of the $HAuCl_4$ slowly produced a yellow precipitate over the span of 20 minutes which was subsequently filtered *in vacuo* using Whatman 44 ashless filter paper. The filter cake was washed twice with 3 mL of Milli-Q water and then washed with 3 mL of diethyl ether. The crude mass obtained after drying *in vacuo* was 1.120 g (91%).

Bis(N,N-di-isopropyldithiocarbamato-S,S′)-gold(III) tetrachloroaurate(III). 1

A small quantity of crude mass was dissolved in a minimum volume of acetone to which hexane was added until cloudy. The cloudy hexane/acetone solution was allowed to crystallise at a reduced temperature. The resultant solid was filtered using Whatmann 44 ashless filter paper and the resultant solid was identified as **1** using NMR and high-resolution mass spectroscopy. ^1H NMR (400.15 MHz, $(CD_3)_2CO$, 295 K): δ 4.74 (sept, $^3J_{HH} = 6.8$ Hz, 4H), 1.59 (d, $^3J_{HH} = 6.8$ Hz, 24H). ^{13}C NMR (100.63 MHz, $(CD_3)_2CO$, 295 K): δ 194.42, 55.71, 19.78. HRMS $(M)^+$ for $[C_{14}H_{28}N_2S_4Au]^+$ Calculated: 549.0795; Found: 549.0788; Error: −1.3 ppm. HRMS $(M)^-$ for $[AuCl_4]^-$ Calculated: 338.8396; Found: 338.8406; Error: 2.9 ppm. UV-Vis ($(CH_3)_2CO$, λ_{max} (nm)): 350, 400, 445. FTIR (ATR, λ cm^{-1}, ν = stretching mode, ρ = rocking mode): 2971 ν (C–H), 1533 ν_s (C···N), 1460 ν_{as} (CH_3), 1447 ν_{sy} (CH_3), 1343 ν (N–C), 1134 ρ (CH_3), 1031 ν_s (C···S).

Dichloro(N,N-di-isopropyldithiocarbamato-S,S′)-gold(III). 2

A small quantity of crude mass was dissolved in a minimum volume of acetone and refluxed for 72 hours. After cooling, hexane was

added until the solution became cloudy. The cloudy hexane/acetone solution was allowed to crystallise at a reduced temperature. The resultant solid was filtered using Whatmann 44 ashless filter paper and the resultant solid was identified as **2** using NMR and high-resolution mass spectroscopy. ^{1}H NMR (400.15 MHz, $(CD_3)_2CO$, 295 K): δ 4.68 (sept, $^{3}J_{HH}$ = 6.8 Hz, 2H), 1.60 (d, $^{3}J_{HH}$ = 6.8 Hz, 12H) ^{13}C NMR (100.63 MHz, $(CD_3)_2CO$, 295 K): δ 190.82, 55.72, 19.78. HRMS $(M)^+$ for $[C_7H_{14}NS_2AuCl_2\text{-}Cl]^+$ Calculated: 407.9916; Found:407.9912; Error: −0.98 ppm. UV-Vis ($(CH_3)_2CO$, λ_{max} (nm)): 350, 395, 437. FTIR (ATR, $\lambda\,cm^{-1}$, ν = stretching mode, ρ = rocking mode): 2975 ν (C–H), 1548 ν_s (C···N), 1451 ν_{as} (CH_3), 1386 ν_{sy} (CH_3), 1343 ν (N–C), 1140 ρ (CH_3), 1029 ν_s (C···S).

Microscopy

Photomicroscopy of the crystal growth process (cross polarised transmission mode) and the electrode surfaces post thermal decomposition of **1** and **2** (brightfield reflectance mode) was performed using a Nikon Eclipse TE200 microscope and photomicrographs were obtained using an Amscope 18 MP-HS USB3.0 Camera. Scanning electron microscopy (SEM) imaging and elemental mapping were conducted using Zeiss Supra 55VP SEM equipped with an Oxford energy dispersive x-ray system. High resolution SEM imaging, EDX, and FIB milling was performed using a Tescan Fera 3 SEM equipped with an Orsay physics iFIB operating at 5 pA current and using Xe plasma. All images were processed using Fiji.[54]

Resistance measurements of thermolysis products

DropSens (Metrohm) interdigitated gold electrodes were loaded with 3–5 mg of **1** and **2** and heated using a highly modified Linkam THMS600 stage enclosed in a high-vacuum chamber which was kept under a positive pressure of 99.9995% Nitrogen gas for these experiments. A Class B Pt100 RTD was adhered to the heating surface using a clamp and used to control the heating rate of the stage. A heating rate of 10 °C min^{-1} from room temperature to 375 °C was achieved using a Linkam TMS 94 controller. The temperature of the interdigitated electrode was evaluated using a Rigol DM3058E digital multimeter and a Class B Pt100 RTD placed within 2 mm of the electrode and held in contact with the heated surface using a clamp. The temperature was calibrated using certified melting point standards (azobenzene, Phenacetin and Saccharin) placed atop an equivalent electrode and heated under equivalent conditions. Electrical resistance measurements were acquired using a Rigol DM3068 electrical multimeter (with a maximum resistance range of 1e^{8} Ω) and a custom LabView VI was used to interface and control the multimeters, and to acquire the temperature and electrical resistance values. Time lapse of the thermal decomposition process was performed using "hyperlapse" functionality of a Samsung Galaxy Fold 4, and the electrode was used to calibrate the scale. Temperature readings within the timelapse were calibrated relative to the end-point of mass loss evaluated from the thermogravimetric analysis and the end point of visual thermal decomposition.

Acknowledgements

Open Access publishing facilitated by Australian Nuclear Science and Technology Organisation, as part of the Wiley - Australian Nuclear Science and Technology Organisation agreement via the Council of Australian University Librarians.

Conflict of Interests

The authors declare no conflict of interest.

Data Availability Statement

The data that support the findings of this study are available in the supplementary material of this article.

Keywords: Dithiocarbamate · gold · microcrystals · thermolysis · single source precursor

[1] M. A. Malik, M. Afzaal, P. O'Brien, *Chem. Rev.* **2010**, ***110***, 4417–4446.
[2] S. Ghosh, B. Dasgupta, C. Walter, P. W. Menezes, M. Driess, *Small Science* **2023**, *3*.
[3] A. Roffey, N. Hollingsworth, G. Hogarth, *Nanoscale Adv.* **2019**, *1*, 3056–3066.
[4] J. C. Sarker, G. Hogarth, *Chem. Rev.* **2021**, ***121***, 6057–6123.
[5] A. Angeloski, M. B. Cortie, J. A. Scott, D. M. Bordin, A. M. McDonagh, *Inorg. Chim. Acta.* **2019**, *487*, 228–233.
[6] A. Angeloski, A. R. Gentle, J. A. Scott, M. B. Cortie, J. M. Hook, M. T. Westerhausen, M. Bhadbhade, A. T. Baker, A. M. McDonagh, *Inorg. Chem.* **2018**, *57*, 2132–2140.
[7] T. Mthethwa, V. S. R. Pullabhotla, P. S. Mdluli, J. Wesley-Smith, N. Revaprasadu, *Polyhedron* **2009**, *28*, 2977–2982.
[8] L. D. Nyamen, V. S. R. Rajasekhar Pullabhotla, A. A. Nejo, P. T. Ndifon, J. H. Warner, N. Revaprasadu, *Dalton Trans.* **2012**, *41 27*, 8297–8302.
[9] A. M. Paca, P. A. Ajibade, *Nanomaterials* **2018**, *8*, 187.
[10] P. Kevin, D. J. Lewis, J. Raftery, M. Azad Malik, P. O'Brien, *J. Cryst. Growth.* **2015**, *415*, 93–99.
[11] A. Roffey, N. Hollingsworth, H. U. Islam, M. Mercy, G. Sankar, C. R. Catlow, G. Hogarth, N. H. de Leeuw, *Nanoscale* **2016**, *8*, 11067.
[12] P. A. Ajibade, J. Z. Mbese, B. Omondi, *Inorg. Nano-Met. Chem.* **2017**, *47*, 202.
[13] B. Arul Prakasam, M. Lahtinen, A. Peuronen, M. Muruganandham, E. Kolehmainen, E. Haapaniemi, M. Sillanpää, *Inorg. Chim. Acta.* **2015**, *425*, 239.
[14] G. Gomathi, S. H. Dar, S. Thirumaran, S. Ciattini, S. Selvanayagam, *C. R. Chim.* **2015**, *18*, 499.
[15] T. Chintso, P. A. Ajibade, *Mater. Lett.* **2015**, *141*, 1.
[16] E. Sathiyaraj, G. Gurumoorthy, S. Thirumaran, *New J. Chem.* **2015**, *39*, 5336.
[17] N. Hollingsworth, A. Roffey, H. U. Islam, M. Mercy, A. Roldan, W. Bras, M. Wolthers, C. R. A. Catlow, G. Sankar, G. Hogarth, N. H. de Leeuw, *Chem. Mater.* **2014**, *26*, 6281.
[18] M. A. Ehsan, T. A. Peiris, K. G. Wijayantha, M. M. Olmstead, Z. Arifin, M. Mazhar, K. M. Lo, V. McKee, *Dalton Trans.* **2013**, *42*, 10919.
[19] G. S. Sivagurunathan, K. Ramalingam, C. Rizzoli, *Polyhedron* **2013**, *65*, 316.
[20] K. Ramasamy, V. L. Kuznetsov, K. Gopal, M. A. Malik, J. Raftery, P. P. Edwards, P. O'Brien, *Chem. Mater.* **2013**, *25*, 266.
[21] P. Li, H. Li, W. Jie, *J. Rare Earth* **2011**, *29*, 317.
[22] I. Jen-La Plante, T. W. Zeid, P. Yang, T. Mokari, *J. Mater. Chem.* **2010**, *20*, 6612.
[23] G. Gurumoorthy, S. Thirumaran, S. Ciattini, *Polyhedron* **2016**, *118*, 143.
[24] D. C. Onwudiwe, P. A. Ajibade, B. Omondi, *J. Mol. Struct.* **2011**, *987*, 58–66.
[25] R. A. Howie, E. R. T. Tiekink, J. L. Wardell, S. M. S. V. Wardell, *J. Chem. Crystallogr.* **2009**, *39*, 293.
[26] J. Cookson, P. D. Beer, *Dalton Trans.* **2007**, *15*, 1459–1472.
[27] Y. Liu, E. R. Tiekink, *CrystEngComm* **2005**, *7*, 20.
[28] R. E. Benson, C. A. Ellis, C. E. Lewis, E. R. T. Tiekink, *CrystEngComm* **2007**, *9*, 930.
[29] F. Nemati, A. Ghorbani Gharjeh Ghiyaei, B. Notash, M. H. Shayegan, V. Amani, *Tetrahedron Lett.* **2014**, *55*, 3572.
[30] G. An, L. Chenguang, Y. Hou, X. Zhang, Y. Liu, *Mater. Lett.* **2008**, *62*, 2643.
[31] C. Schliebe, K. Jiang, S. Schulze, M. Hietschold, W.-B. Cai, H. Lang, *Chem. Commun.* **2013**, *49*, 3991–3993.

[32] A. Tuchscherer, D. Schaarschmidt, S. Schulze, M. Hietschold, H. Lang, *Inorg. Chem. Commun.* **2011**, *14*, 676–678.
[33] S. Komiya, T. Sone, S. Ozaki, M. Ishikawa, N. Kasuga, *J. Organomet. Chem.* **1992**, *428*, 303–313.
[34] D. Zopes, C. Hegemann, J. Schlafer, W. Tyrra, S. Mathur, *Inorg. Chem.* **2015**, *54*, 3781–3787.
[35] J. Zhang, Y. Gao, R. A. Alvarez-Puebla, J. M. Buriak, H. Fenniri, *Adv. Mater.* **2006**, *18*, 3233–3237.
[36] T. Masaharu, M. Nobuhiro, N. Michiko, H. Sachie, I. Naoki, *B. Chem. Soc. Jpn.* **2007**, *80*, 2024–2038.
[37] C. J. Rodrigues, J. A. Bobb, M. G. John, S. P. Fisenko, M. S. El-Shall, K. M. Tibbetts, *Phys. Chem. Chem. Phys.* **2018**, *20*, 28465–28475.
[38] X. Lu, H. Y. Tuan, B. A. Korgel, Y. Xia, *Chemistry* **2008**, *14*, 1584–1591.
[39] A. E. Turgambaeva, G. Zharkova, P. Semyannikov, V. V. Krisyuk, T. Koretskaya, S. Trubin, B. Kuchumov, I. Igumenov, *Gold Bull.* **2011**, *44*, 177–184.
[40] R. G. Parkhomenko, A. E. Turgambaeva, N. B. Morozova, S. V. Trubin, V. V. Krisyuk, I. K. Igumenov, *Chem. Vap. Deposition* **2013**, ***19***, 38–44.
[41] R. G. Parkhomenko, S. V. Trubin, A. E. Turgambaeva, I. K. Igumenov, *J. Cryst. Growth.* **2015**, *414*, 143–150.
[42] M. Mäkelä, T. Hatanpää, K. Mizohata, J. Räisänen, M. Ritala, M. Leskelä, *Chem. Mater.* **2017**, *29*, 6130–6136.
[43] C. L. Teske, A.-L. Hansen, R. Weihrich, L. Kienle, M. Kamp, K. P. van der Zwan, J. Senker, C. Dosche, G. Wittstock, W. Bensch, *Chem. Eur. J.* **2019**, *25*, 6763–6772.
[44] G. I. Zharkova, I. A. Baidina, I. K. Igumenov, *J. Struct. Chem.* **2007**, *48*, 108–113.
[45] I. A. Lutsenko, A. V. Ivanov, M. A. Kiskin, G. V. Ogil'ko, *Russ. J. Inorg. Chem.* **2015**, *60*, 92–99.
[46] A. V. Ivanov, O. V. Loseva, T. A. Rodina, A. V. Gerasimenko, E. V. Novikova, *Russ. J. Coord. Chem.* **2016**, *42*, 104–115.
[47] O. V. Loseva, T. A. Rodina, A. V. Ivanov, I. A. Lutsenko, E. V. Korneeva, A. V. Gerasimenko, A. I. Smolentsev, *Russ. J. Coord. Chem.* **2018**, *44*, 604–612.
[48] A. Angeloski, A. Rawal, M. Bhadbhade, J. M. Hook, R. W. Schurko, A. M. McDonagh, *Cryst. Growth Des.* **2019**, *19*, 1125–1133.
[49] K. Otto, I. Oja Acik, M. Krunks, K. Tõnsuaadu, A. Mere, *J. Therm. Anal. Calorim.* **2014**, *118*, 1065–1072.
[50] T. A. Rodina, A. V. Ivanov, A. V. Gerasimenko, O. V. Loseva, O. N. Antzutkin, V. I. Sergienko, *Polyhedron* **2012**, *40*, 53–64.
[51] J. K. Lee, D. Samanta, H. G. Nam, R. N. Zare, *Nat. Commun.* **2018**, *9*, 1562.
[52] B. Radha, G. U. Kulkarni, *Cryst. Growth Des.* **2011**, *11*, 320–327.
[53] S. R. King, J. Massicot, A. M. McDonagh, *Metals* **2015**, *5*, 1454–1461.
[54] J. Schindelin, I. Arganda-Carreras, E. Frise, V. Kaynig, M. Longair, T. Pietzsch, S. Preibisch, C. Rueden, S. Saalfeld, B. Schmid, J.-Y. Tinevez, D. J. White, V. Hartenstein, K. Eliceiri, P. Tomancak, A. Cardona, *Nat. Methods* **2012**, *9*, 676–682.

Manuscript received: October 26, 2023
Revised manuscript received: November 28, 2023
Accepted manuscript online: December 6, 2023
Version of record online: February 1, 2024